Journal of
Marine Science and Engineering

Article

The Control-Oriented Heat Release Rate Model for a Marine Dual-Fuel Engine under All the Operating Modes and Loads

Yuanyuan Tang *, He Li, Yuchi Jiang, Wenwei Liang and Jundong Zhang

Marine Engineering College, Dalian Maritime University, Dalian 116000, China
* Correspondence: tangpaper2022@163.com

Abstract: An accurate model plays an important role in control strategy development of smart ships. For the control-oriented engine models, calibration by experienced personnel is key to outputting high accuracy. However, the dual-fuel engine runs in liquid fuel mode, gas fuel mode, and fuel sharing mode. It is impossible to tune a single model or a set of parameters for the dual-fuel engine under all operating modes and loads. On the basis of our experience and practice, a Wiebe-based heat release rate model is used. To make the Wiebe model available for the dual-fuel engine, the Wiebe parameters are assumed to be linear functions. The combustion beginning angle is modeled as a function of fuel quantity in liquid fuel mode and as a look-up table in gas fuel mode for all loads. The combustion duration and the combustion distribution factor are modeled as a function of fuel quantity and engine revolution both in liquid fuel mode and in gas fuel mode. In fuel sharing mode, the heat release rate is modeled as a combination of the heat release rate models in liquid fuel mode and gas fuel mode. This model is called the SL model. For a further discussion, four types of combinations in fuel sharing mode are investigated. In addition, in liquid fuel mode and gas fuel mode, the combustion duration model and the combustion distribution factor model are replaced by the Woschni/Anisits model, which was specifically used in the diesel engine. This variation of model is called the WA model. To validate our hypothesis and models, the Wiebe parameters in liquid fuel mode and gas fuel mode are given, four types of combinations and two cases of comparisons in fuel sharing model are discussed, and the engine performance is checked and analysed. Results show that for the SL model, the average RMSE is 1.45% in the liquid fuel mode, 2.22% in the gas fuel mode, and 2.53% in the fuel sharing mode. For the WA model, the RMSE of the NOx is 9.79% in liquid fuel mode and 45.20% in gas fuel mode. Its maximum error reaches −65.54%. The proposed SL model is accurate and can generate Wiebe parameters that are better than the carefully tuned parameters. The WA model is not suitable for engine models that require NOx-emission-related parameters.

Keywords: Wiebe; dual-fuel engine; heat release rate; engine model; Woschni

check for updates

Citation: Tang, Y.; Li, H.; Jiang, Y.; Liang, W.; Zhang, J. The Control-Oriented Heat Release Rate Model for a Marine Dual-Fuel Engine under All the Operating Modes and Loads. *J. Mar. Sci. Eng.* **2023**, *11*, 64. https://doi.org/10.3390/jmse11010064

Academic Editor: Dong-Sheng Jeng

Received: 7 November 2022
Revised: 28 December 2022
Accepted: 29 December 2022
Published: 2 January 2023

1. Introduction

In the section of marine transportation, the NG-diesel dual-fuel engine is one of the most popular engines for ocean-going vessels and river vessels due to its cleaner emission and significant economic benefit in LNG carriers. Against the background of reducing 50% of GHG (greenhouse gas) emissions from the shipping industry by 2050, improving energy efficiency is one of the hot spots [1]. To improve energy efficiency, an accurate dual-fuel engine model is one of the key factors since the control strategy greatly affects energy efficiency. The widely accepted control-oriented engine models are specified for liquid diesel oil with direct injection or liquid gasoline with port injection. MAN 51/60DF dual-fuel engine can burn natural gas and diesel oil and can run in liquid fuel mode, gas fuel mode, and fuel sharing model. Its complexity makes the heat release rate difficult to calculate. It is the core sub-model in the engine model. Thus, we propose a Wiebe-based heat release rate model. It can be used to calculate the heat release rate for the dual-fuel engine.

The heat release rate is one of the key parameters of combustion, but it could not be measured directly up to now. One way to obtain its value is to calculate it from the measured in-cylinder pressure according to the thermal dynamic theory [2,3]. The other way to obtain its value is to calculate it from the combustion model. Over decades of development, there are various types of combustion models, such as the fractal-based combustion model [4], the mixing-controlled combustion (MCC) model for DI diesel engines [5,6], the quasi-dimensional combustion models [7,8], and the Wiebe empirical model [9]. The fractal-based combustion model assumes that the main part of the heat release is due to the turbulent premixed flame propagation. It considers the flame front to be a wrinkled spherical surface centered in the spark plug location. The rate of heat release is the rate of flame front propagation. By describing the physics of the small scales of turbulence on the basis of the phenomenological concept of vortex cascade and fractal theory, the fractal-based combustion model can simulate both premixed and non-premixed turbulent flames [10]. MCC considers the DI diesel engine combustion as the combination of premixed-controlled combustion and diffusion-controlled combustion. For the premixed-controlled combustion, the rate of heat release is determined by the rate of chemical kinetic reaction. It is correlated by a Wiebe function. For the diffusion combustion, the rate of heat release relies on the rate of fuel–air mixing and is a function of the available fuel quantity and the turbulent kinetic energy density. The representative quasi-dimensional models are the Cummins gaseous jet model and the Hiroyasu oil droplet model. The Hiroyasu oil droplet model divides the spray into zones in the radial and axial directions and tracks the evolution of the packets over time. In each packet, only fuel vapor reacts with the surrounding air. The fuel droplets in liquid state are not ready for combustion. The mass of fuel burned in a packet is determined by the mass of fuel vapor and air. It is limited by the chemical reaction rate [11]. The Wiebe empirical model considers that the rate of heat release can be directly correlated by combustion duration, combustion start crank angle, and a combustion rate distribution factor (also called combustion shape parameter). The Wiebe model discards the complex combustion distribution in space and in time. It keeps the key factors and simplifies the three-dimensional properties into zero-dimension. Since the Wiebe model is an empirical model, it can be used for various types of engines and fuel types. With fine calibration, it can generate excellent accuracy. When it is used in a 0D diesel engine model, it can also meet the real-time requirement. Tang, Y. [12] optimized the in-cylinder process and obtained the real-time execution of a marine low speed diesel engine.

The phenomenology combustion models are too complex for control applications. Some of the parameters are difficult to determine. Generally, these models are developed for specified engine types, and they are sensitive to the fuel types. The Wiebe model is the most widely used model due to its simple form, fast calculation speed, and nonsensitivity to fuel types and engine types [9]. It has already been widely used in advanced combustion concept analyses, such as the HCCI [13,14], RCCI [15], and PPC [16], in alternative fuel investigations, such as the biodiesel [17] and hydrogen [18,19], in control strategy developments, such as the injection strategy [16,20] and phasing control [21–23], in knocking avoidance [19,24], in fault diagnosis [25], in propulsion system dynamics research [26], in hydraulic-free piston engine [27], and so on. Sui, W. B. [21–23] developed a control-oriented model for a dual-fuel engine and an engine with VGT and EGR to test their adaptive control strategy and feedforward control strategy for combustion phasing control. In their model, the Wiebe model is used to predict the CA50. Liu, J. L. [28,29] compared the model performance in peak firing pressure, mass fraction of burned fuel, and heat release rate using a single Wiebe, a double Wiebe, and a triple Wiebe for the natural-gas-spark-ignited diesel engine. It concluded that the triple Wiebe was more suitable for his research engine. Xiang, L. [24] used a zero-dimension two-zone model and a Wiebe heat release rate model to investigate the effects of compression ratio, air–fuel equivalence ratio, and ignition timing on the knocking performance of a spark ignition natural gas engine. They also investigated the effect of pilot fuel energy on the knocking performance of a compression ignition dual-fuel engine. Sapra, H. [18] compared the performance of the Seiliger model and double-Wiebe model on a spark ignition hydrogen–natural-gas engine. This work showed that the Wiebe model has poor prediction capability. Diaz, G. J. A. [19] investigated the effects of hydrogen and methane proportions, compression ratio, and equivalence ratio on the knock occurrence crank angle, the combustion duration, and the compression polytropic coefficient in a cooperative fuel research engine. The mass fraction of burned fuel was fitted with a Wiebe function. Kozlov, A. [30] investigated the effect of pilot fuel mass, pilot fuel injection pressure, pilot fuel injection timing, and excess air ratio on the combustion process of a heavy-duty dual-fuel diesel-ignited gas engine. The Wiebe model was used for heat release rate calculation at each operating point. From these fellow works, it can be seen that the Wiebe model is still active and is so widely used.

MAN 51/60DF combines the port injection and direct injection and the gas fuel and the liquid fuel in one. This fact prevents the existing combustion models from being used directly for the engine's overall performance calculation. As an inborn drawback of the Wiebe model, each set of parameters corresponds solely to an engine load. It cannot be used in all modes and loads. To overcome this drawback, much research work has been carried out. Mikulski, M. [31,32] created a fast and reliable dual-fuel combustion model to be used for model-based control development. The diesel burning rate was fitted by a Wiebe-based function. It was modified as the linear relationship of combustion duration with fuel oil consumption. The gaseous fuel combustion was modeled as single-step macro-reaction kinetics. Loganathan, S. [33] used a Wiebe function to investigate the heat release rate of a DME-fueled diesel engine. All Wiebe parameters were modified by LCF (load correction factor) and OCF (oxygenate correction factor). LCF is the ratio of diesel mass flow rates between the optimum load and others. OCF is the ratio of mass flow rates between DME and diesel at identical power output. Yang, T. H. [16] used a linear algorithm to identify the double-Wiebe parameters so that it could be used to optimize the fuel injection and achieved the benefits of partially premixed combustion. Stoumpos, S. [34] used a database to store the parameters of the triple-Wiebe function. Christopher Kim Blomberg [35] used a three-stage heat release model to investigate the HCCI combustion performance. It combines LTR (low temperature heat release), ITR (intermediate temperature heat release), and HTR (high temperature heat release) into one model. The LTR and HTR are Wiebe functions. The ITR is a Wiebe-like exponential function. Sedigheh Tolou [36] used a double-Wiebe function to account for the rapid initial premixed combustion and a gradual diffusion-like state of combustion for a GDI engine. Variables of the Wiebe function were correlated to derive a predictive combustion model.

Researchers, in addition to those mentioned above, have conducted much research on the combustion model development, but there is a lack of a control-oriented models that can calculate the overall performance of the dual-fuel engine under all operating modes and loads. The Wiebe model will be one of the most suitable candidates for the control-oriented heat release rate model of the dual-fuel engine. As it can only be used in a load, the Woschni/Anisit model was specified for diesel engines, and an unnamed model was specified for gasoline engines to extend the load range of the Wiebe model. However, there is no publicly acceptable solution for dual-fuel engines. In addition, there are two more factors, the fuel type and the fuel ratio, introduced into the dual-fuel engine model. This makes the dual-fuel engine model more complex. To solve this problem, the SL (standard linear) model is proposed. It correlates the Wiebe parameters on the basis of the linear functions in liquid fuel mode and gas fuel mode. In fuel sharing mode, it combines the model in liquid fuel mode and that in gas fuel mode. Four types of combinations in fuel sharing mode and replacement by Woschni/Anisit model in liquid fuel mode and gas fuel mode are further discussed. Results show that the SL model is accurate for the dual-fuel engine. It makes the dual-fuel engine simulation in all operating modes and loads possible with only a single model and a single set of parameters.

In this paper, the specifications and attributes related to our study of the dual-fuel engine are introduced first. Then, the modeling hypothesis and definition of the proposed model are presented. The next three sections present the process and result of the model validation and discussion. Finally, a summary and a conclusion are given. The hypothesis and the proposed model are proven to be feasible and applicable.

2. Engine Specifications

The engine used for investigation is MAN 51/60DF. The specifications are shown in Table 1. It is a four-stroke dual-fuel engine with a natural gas injector at the intake pipe, a main diesel injector at the center of the cylinder head, and an ignition diesel injector near the main diesel injector. The main diesel injector is cam-controlled with a VIT mechanism. The natural gas injector and the ignition diesel injector are electronically controlled. It can work in liquid fuel mode, gas fuel mode, fuel sharing mode, and backup mode. In liquid fuel mode, the main diesel injector and ignition diesel injector are enabled. The ignition diesel injector is activated for clogging prevention. In gas fuel mode, the natural gas injector and ignition diesel injector are enabled. In fuel sharing mode, all the injectors are activated. The engine in backup mode is the same as a diesel engine.

Table 1. Specifications of the dual-fuel engine under study (100% load).

Parameter	Value
Cylinder number (-)	8, line
Cylinder diameter (mm)	510
Cylinder stroke (mm)	600
Compression ratio (-)	13.3
Rated power (kW)	8000
Rated speed (rpm)	514
Peak pressure (MPa)	14.3
MEP (Mpa)	1.91
SFOC (g/kWh)	189.1
Fire order (-)	1-4-7-6-8-5-2-3
Working mode (-)	Liquid fuel mode, gas fuel mode, fuel sharing mode, backup mode

3. Ideas for the SL Model and Validation

The general single-Wiebe heat release rate model is shown in Equation (1). For a specified type of engine and fuel, parameters in the Wiebe function are different in different loads. A set of parameters can only be used in a load.

$$\frac{dx}{d\varphi} = 6.908\frac{(d+1)}{\varphi_z}\left(\frac{\varphi-\varphi_B}{\varphi_z}\right)^d \exp\left[-6.908\left(\frac{\varphi-\varphi_B}{\varphi_z}\right)^{d+1}\right] \tag{1}$$

To extend the Wiebe model to different loads, Woschni, G. and Anisit, F. modified the combustion duration φ_z and combustion distribution factor d for the diesel engine, as shown in Equations (2) and (3). This model requires a set of validated parameters as the reference values.

$$\varphi_z = \varphi_{z0}\left(\frac{\alpha_0}{\alpha}\right)^{0.6}\left(\frac{n}{n_0}\right)^{0.5} \tag{2}$$

$$d = d_0\left(\frac{\tau_{ID_0}}{\tau_{ID}}\right)^{0.6}\left(\frac{p}{p_0}\right)\left(\frac{T_0}{T}\right)\left(\frac{n}{n_0}\right)^{0.3} \tag{3}$$

The subscript 0 denotes the reference parameters, and they have been well validated. α is the air–fuel ratio; n is the revolution speed; τ_{ID} is the ignition delay; and p and T are the pressure and temperature at the compression beginning, respectively.

In the quasi-dimensional combustion model, the fuel combustion rate is proportional to the fuel concentration and oxygen concentration, as shown in Equation (4).

$$\frac{dm_f}{dt} = A_d \exp\left(-\frac{E_a}{RT}\right)[\mathrm{C}_{12}\mathrm{H}_{26}]^{0.25}[\mathrm{O}_2]^{1.5} V_{pac} M_{fuel} \quad (4)$$

It can be inferred from Equation (4) that more time is needed when there is more fuel that needs to be burned. Discarding the complex processes during combustion, we suppose that the duration of combustion depends mainly on the amount of injected fuel. If the duration is expressed in terms of crank angle, the combustion duration can be directly derived from the revolution speed, as shown in Equation (5).

$$\varphi_z[\mathrm{CA}] = 360^{\mathrm{o}} \times \frac{n[\mathrm{r/min}]}{60[\mathrm{s/min}]} \times t[\mathrm{s}] \quad (5)$$

Therefore, the combustion duration can be regarded as the function of the amount of fuel injected into each cylinder and the revolution speed of crankshaft, as shown in Equation (6).

$$\varphi_z = \varphi_{z0} \times f\left(m_f, n\right) \quad (6)$$

In gas fuel mode, the fuel gas and air are well mixed. Thus, its combustion rate is limited by the rate of chemical reaction. Compared with the liquid fuel mode, since there is no fuel vapor preparation, the combustion duration in gas fuel mode will be shorter. The angle difference is assumed to be a constant value at the same load. Thus, the combustion duration in gas fuel mode can be derived from the value in liquid fuel mode, as shown in Equation (7).

$$\varphi_z = \varphi_{z0} \times f\left(m_f, n\right) - \Delta\varphi \quad (7)$$

As the engine runs at a fixed speed, it has almost the same injection pressure. Therefore, the injected fuel per crank angle can be considered equal at different loads. The injection duration is longer than the ignition delay. During the ignition delay, the amount of injected fuel per crank angle at low load and heavy load is almost equal. Then, the amount of fuel vapor after injection can be considered to vary only with the thermal history of compression. The thermal history of compression can be measured by the integral of the in-cylinder temperature from the beginning of compression to the beginning of combustion. The total injected fuel is varied with different loads. When the combustion rate distribution is described in crank angle, it will additionally be affected by the engine revolution speed. In summary, the combustion distribution factor can be affected by the thermal history during the compression, the total injected fuel, and the revolution speed, as shown in Equation (8).

$$d = d_0 \times f\left(T, m_f, n\right) \quad (8)$$

In gas fuel mode, assuming a similar combustion rate at the beginning of combustion from light load to heavy load, the ratio of burned fuel at the beginning will be smaller at heavy load than that at light load. Therefore, the combustion distribution factor will be smaller at a heavy load than at a light load. As the combustion duration is shorter and the combustion rate is greater in gas fuel mode, the combustion distribution factor will be smaller in this mode. Thus, the combustion distribution factor in gas fuel mode can be described in Equation (9).

$$d = d_0 \times f\left(T, m_f, n\right) - \Delta d \quad (9)$$

The ignition delay τ_{ID} is defined as the crank angle interval from the fuel injection to the beginning of combustion. Thus, the angle of combustion beginning can be derived from injection timing and ignition delay, as shown in Equation (10).

$$\varphi_b = \varphi_i + \tau_{ID} \quad (10)$$

The timing of fuel injection is controlled by the fuel pump in liquid fuel mode. The timing of ignition oil injection is controlled by ECU in gas fuel mode. The value of combustion beginning angle will be regular in liquid fuel mode and will be irregular in gas fuel mode. When the engine load increases from light to heavy, the internal energy of the working medium gradually increases during the compression process. The higher compression temperature results in more rapid evaporation after fuel injection. Thus, the suitable fuel vapor for auto-ignition will be formed in a shorter time at heavy load. Considering the same injection timing, the combustion beginning angle will be advanced, according to Equation (10). Thus, the combustion beginning angle can be modeled as a function of engine load, as shown in Equation (11).

$$\varphi_b = \varphi_{b0} \times f(P_{load}) \tag{11}$$

For the fuel sharing model, the three Wiebe parameters are assumed to be a linear combination of the values in liquid fuel mode and gas fuel mode. On the basis of these assumptions, the parameter models of the dual-fuel engine can be established, as shown in Equations (12)–(14).

$$\varphi_z = k_1 \times \varphi_{z0} \times f_1\left(m_f, n\right) + (1 - k_1) \times \left[\varphi_{z0} \times f_1\left(m_f, n\right) - \Delta\varphi\right] \tag{12}$$

$$d = k_2 \times d_0 \times f_2\left(T, m_f, n\right) + (1 - k_2) \times \left[d_0 \times f_2\left(T, m_f, n\right) - \Delta d\right] \tag{13}$$

$$\varphi_b = k_3 \times f_{3l}(P_{load}) + (1 - k_3) \times f_{3g}(P_{load}) \tag{14}$$

As the engine runs at a constant speed, the effect of speed at different loads can be neglected. For the four-stroke medium speed engine, the effect of the temperature history on the combustion distribution factor during the compression will be much less than the effect of the quantity of burned fuel. For the constant speed engine, the engine power is directly related to the injected fuel, and it is nearly a linear relationship. Thus, we assumed these functions are linear. Then, the parameter models of the dual-fuel engine can be rewritten, as shown in Equations (15)–(17). This model is called the SL model.

$$\varphi_z = k_1 \times \varphi_{z0} \times \left(a_1 \frac{m_f}{m_{f0}} + b_1\right) + (1 - k_1) \times \left[\varphi_{z0} \times \left(a_1 \frac{m_f}{m_{f0}} + b_1\right) - \Delta\varphi\right] \tag{15}$$

$$d = k_2 \times d_0 \times \left(a_2 \frac{m_f}{m_{f0}} + b_2\right) + (1 - k_2) \times \left[d_0 \times \left(a_2 \frac{m_f}{m_{f0}} + b_2\right) - \Delta d\right] \tag{16}$$

$$\varphi_b = k_3 \times f_{3l}(P_{load}) + (1 - k_3) \times f_{3g}(P_{load}) \tag{17}$$

To validate our proposition, a zero-dimensional two-zone model is used. As the focus is on the heat release rate model, the engine cylinders, intake manifold, and exhaust manifold are modeled only on AVL BOOST, and the turbocharger model is omitted. The combustion-related performance parameters, such as the thermal parameters and NOx emissions, are included. The air cooler outlet cross-section and the turbine inlet cross-section are selected as the inlet and outlet boundaries, respectively. Since the exhaust manifold temperature is not measured in the shop test, the turbine inlet temperature is used instead. The details of engine modeling can be found in our previous work and peer literature [12,37–40]. The 100% load is selected as the reference load. For a further discussion, four types of combinations in fuel sharing mode and replacement of the correlation function are studied. The idea for this study is presented in Figure 1.

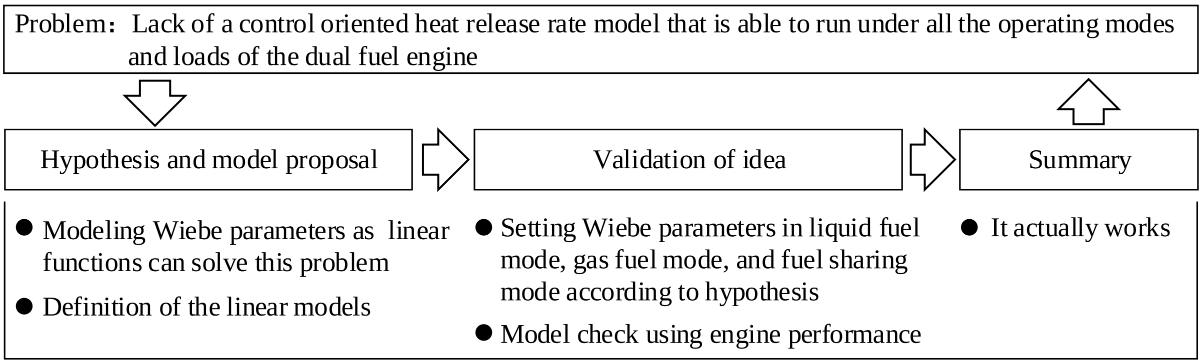

Figure 1. Overview of the idea and scheme.

4. Model Validation in Liquid Fuel Mode

4.1. Wiebe Parameters according to the SL Model

In order to validate our assumption, the Wiebe parameters for dual-fuel engine running in liquid fuel mode are given in Table 2. They are given according to our experience in model calibration and the rules we analyzed above. In Table 2, the crank angle at the top dead center is defined as zero. $\varphi_b{}'$ is the value without the correction of VIT.

Table 2. The Wiebe parameters according to the SL model in liquid fuel mode.

Load (%)	25	50	75	85	100	110
$\varphi_b{}'$ (deg CA)	−2	−3	−4	−4.4	−5	−5.4
VIT (deg CA)	0	+4	+4	0	0	0
φ_b (deg CA)	−2	1	0	−4.4	−5	−5.4
φ_z (deg CA)	30	40	50	54	60	64
d (-)	1.5	1.4	1.3	1.26	1.2	1.16

The fuel injection system of the dual-fuel engine contains a variable injection timing (VIT) mechanism. According to the engine test report approved by LR (Lloyd's Register of Shipping), CCS (China Classification Society), and RINA (Registro Italiano Navale), the VIT reading values are −20 at 50% load and 75% load and +40 at 25% load, 85% load, 100% load, and 110% load. Although the actual crank angle corresponding to the VIT value is not known, it is certain that the 25% load, 85% load, 100% load, and 110% load have the same injection timing, and the 50% load and 75% load also have the same injection timing. The difference in VIT values is 60. If +4 crank angles are assumed to correspond to the 60 VIT value, then the combustion beginning angles at 50% load and 75% load should be −3 and −4, respectively.

4.2. Performance Validation of the SL Model

Since the SL model is specified for the dual-fuel engine performance calculation, the performance of the engine is used for the validation of the SL model. The performance of the engine model is given in Table 3 and Figure 2. In Table 3, M stands for the measured value, C stands for the calculated values, m_f is the single-cylinder injected fuel per cycle, P is the engine shaft power, $p_{\max}$ is the peak fire pressure, $\dot{m}_a$ is the intake air flow rate, T_e is the exhaust gas outlet temperature, T_m is the exhaust manifold temperature, and $\dot{m}_n$ is the NOx-specific mass flow rate. The symbol E is the error between the calculated value and the measured value, as Equation (18) shows.

$$E = \frac{C - M}{M} \times 100\% \tag{18}$$

Table 3. The performance of the dual-fuel engine running in liquid fuel mode with the SL model.

Load (%)		**25**	**50**	**75**	**85**	**100**	**110**	**RMSE**
m_f (g)	*M*	3.68	6.57	9.47	10.31	12.27	13.74	
	C	3.68	6.57	9.47	10.61	12.27	13.74	
	E	0.00	0.00	0.00	2.90	0.00	0.00	1.19
P (kW)	*M*	1999	4014	6005	6802	8004	8809	
	C	2024	4025	6010	6938	7997	8844	
	E	1.23	0.28	0.08	2.00	−0.09	0.40	0.98
$p_{\max}$ (bar)	*M*	56	77	107	129	142	149	
	C	57.6	79.0	107.4	129.1	144.1	153.5	
	E	1.05	1.28	−0.56	−0.69	0.77	2.33	1.26
$\dot{m}_{\mathrm{az}}$ (kg/s)	*M*	4.75	9.17	13.66	-	16.02	-	
	C	4.89	9.26	13.82	14.49	16.40	17.32	
	E	2.78	0.96	1.16	-	2.38	-	2.04
T_e (K)	*M*	670	656	666	672	702	733	
	C	696	666	651	664	708	712	
	E	3.88	1.57	−2.22	−1.15	0.90	−2.86	2.34
T_m (K)	*M*	754	734	741	747	782	818	
	C	745	729	731	748	771	795	
	E	−1.19	−0.69	−1.30	0.08	−1.43	−2.81	1.51
$\dot{m}_n$ (g/kWh)	*M*	16.72	9.04	8.90	-	11.02	-	
	C	16.68	9.15	8.98	17.87	11.08	15.96	
	E	−0.21	1.21	0.95	-	0.51	-	0.81
RMSE		2.00	1.00	1.16	1.70	1.15	2.08	

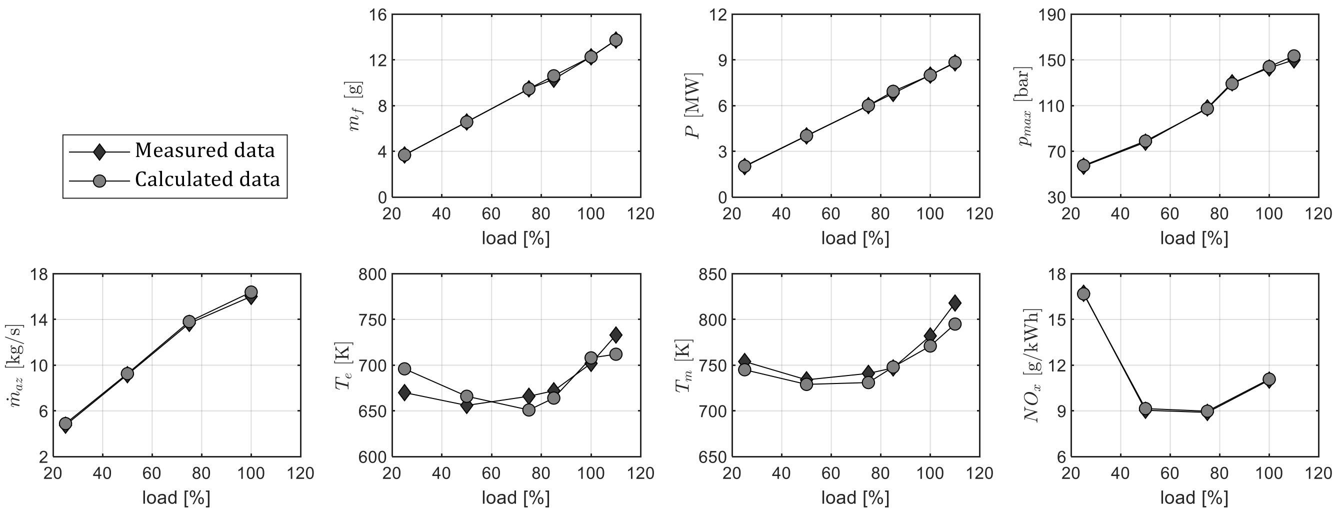

Figure 2. The performance of the dual-fuel engine running in liquid fuel mode with the SL model.

The RMSE is the root mean square error. It is defined in Equation (19).

$$\mathrm{RMSE} = \sqrt{\frac{1}{\mathrm{n}}\sum\left(\frac{C-M}{M}\times 100\%\right)^2} \quad (19)$$

In Table 3, the measured value of the pressure is the gauge pressure. The calculated value of the pressure is the absolute pressure. For the calculation of the error and the RMSE, the gauge pressure is converted to the absolute pressure by adding one atmospheric pressure.

According to the data in Table 3, it shows excellent overall performance. For all the parameters, their errors are within ±4% in all the considered loads, and many are even within ±1%. All the calculated parameters are accurate. According to Figure 2, it can be seen that the injected fuel per cylinder m_f, the engine shaft power P, the peak firing pressure $p_{\max}$, and the intake air flow rate $\dot{m}_a$ are nearly linearly varied with the engine load. However, the calculated exhaust gas outlet temperature T_e is poorer in value prediction than the other parameters. However, the calculated exhaust manifold temperature T_m shows higher accuracy than T_e in both trend prediction and value prediction. In an intuitive sense, the T_m and the T_e should have similar accuracy since the exhaust gas entering the exhaust manifold is the same gas. In fact, the exhaust gas temperature is difficult to model. For two-stroke and four-stroke engines, the exhaust process occupies only a portion of an engine cycle, approximately 40%. During this period, the exhaust gas temperature changes rapidly, but the temperature measured by sensor lags far behind the actual temperature because of the existence of thermal inertia. At the same time, a portion of the internal energy is converted to the kinetic energy near the place of the exhaust temperature sensor. Then, this portion of kinetic energy is converted back to internal energy at the exhaust manifold. It is a challenge for a model to truly play back the heat exchange process between the temperature sensor and its surrounding gas. The calculation method is not given in BOOST. However, there are generally three methods for calculating the exhaust gas temperature, namely the time-based average temperature model, the flow-based average temperature model, and the energy-based average temperature model. The exhaust gas temperatures calculated by the three models are inconsistent with each other and have a certain deviation from the measured exhaust gas temperature.

According to the above analysis, the calculated performance of the engine model using the SL model is generally well matched with the actual engine performance. It demonstrates that the SL model is suitable for control-oriented dual-fuel engine models.

To give insight into the heat release of the dual-fuel engine, the curves of heat release distribution and the heat release rate at 25%, 50%, 75%, and 100% load are presented in Figure 3. In this figure, the heat release rate curve is the product of Wiebe function and injected fuel per cylinder. The combustion beginning of all the curves is shifted to the zero crank angle.

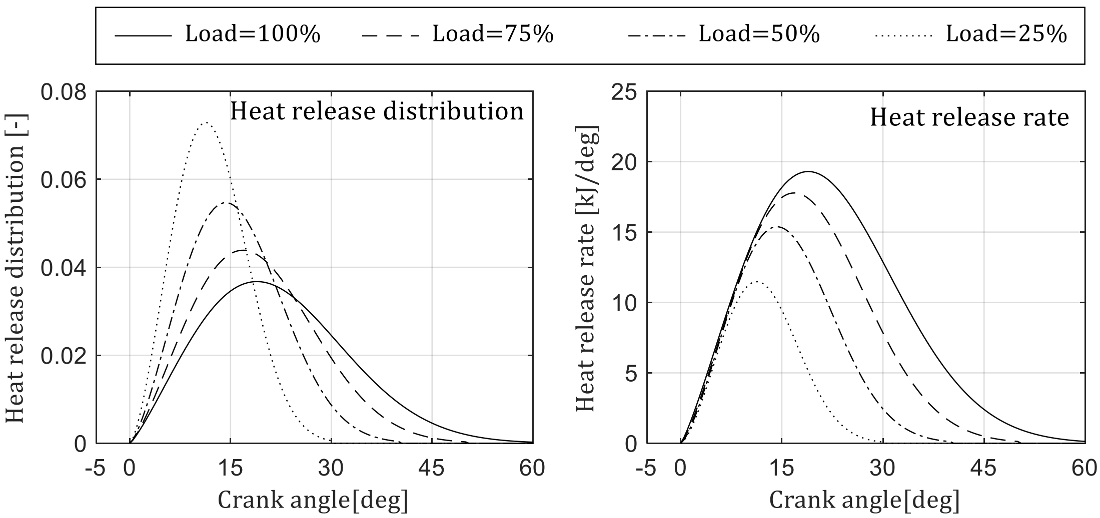

Figure 3. The heat release characteristics of the engine in liquid fuel mode with the SL model.

According to the curves of heat release distribution, it can be seen that as the load increases, the peak value of the curve decreases, but the rate of decline slows down. It can also be seen that the rate of fuel-burned mass to the total mass in the early combustion decreases when the load increases. This is because there is more fuel that needs to be burned at heavy loads. According to the curves of the heat release rate, it can be seen that as the load increases, the maximum value increases and occurs later. However, the heat release rate at the early crank angle remains almost constant for all the loads. These characteristics of this heat release model are consistent with the actual trend.

4.3. Further Discussion of the Woschni/Anisits Model

In order to further investigate the performance of the Woschni/Anisits model (WA model), the Wiebe parameters are also calculated using the WA model, as shown in Table 4. The 100% load is the reference load. From the data in Table 4, it can be seen that the calculated combustion duration is inconsistent with the actual trend and has no obvious regularity. The combustion distribution factor is almost linear with the engine load.

Table 4. The Wiebe parameters according to the WA model in liquid fuel mode.

Load (%)	**25**	**50**	**75**	**85**	**100**	**110**
α (-)	2.58	2.74	2.84	2.66	2.60	2.45
p (bar)	1.30	2.20	3.29	3.46	3.95	4.18
T (K)	385	353	357	358	358	359
τ_{ID_0}/τ_{ID} (-)	1	1	1	1	1	1
φ_b (CA)	−2	1	0	−4.4	−5	−5.4
φ_z (CA)	60.3	58.1	56.9	59.2	60.0	62.2
d (-)	0.37	0.68	1.00	1.05	1.20	1.27

In Table 4, the air–fuel equivalence ratio is calculated by the air mass flow rate and fuel equivalent air mass flow rate, as Equation (20) shows.

$$\alpha = \frac{\dot{m}_a}{\dot{m}_f \times 15.0} \tag{20}$$

Since there are no measured values for the pressure and the temperature at the beginning of compression, the calculated values from the dual-fuel engine model are used instead. As the calculation for ignition delay will introduce other parameters and there is no widely accepted model, the ratio of ignition delay is set to 1. The WA model has no method to calculate the combustion beginning angle. It retains the same values as the SL model.

In order to test the performance of the WA model, the same engine model is used, but the Wiebe parameters are derived from the WA model. All the factors in the engine model remain the same as that in the SL model. Results are shown in Table 5.

From the view of the parameters at single load, the maximal error of the power prediction is 1.62% at 85% load. It is −3.16% for the peak firing pressure at 25% load, 2.68% for the mass flow rate at 25% load, 4.84% for the exhaust gas temperature at 25% load, −4.12% for the exhaust manifold at 110% load, and 13.09% for the NOx emission at 25% load. The mass of injected fuel is the input parameter. Its value is assigned.

From the view of the RMSE of each parameter, the NOx emission has the maximum RMSE, approximately 9.79. The second is the exhaust gas temperature, approximately 2.62. Then, it is the exhaust manifold temperature, approximately 2.26. The RMSE of mass flow rate from the intake manifold to the cylinder is 1.94, and the RMSE of peak firing pressure is 1.75. Additionally, the RMSE of the engine power is 0.91. From the data, it can be seen that the NOx emission has the maximum error. This is caused directly by the temperature difference in the cylinder and indirectly by the heat release rate.

Table 5. The performance of the dual-fuel engine running in liquid fuel mode with the WA model.

Load (%)		**25**	**50**	**75**	**85**	**100**	**110**	**RMSE**
m_f (g)	M	3.68	6.57	9.47	10.31	12.27	13.74	
	C	3.68	6.57	9.47	10.61	12.27	13.74	
	E	0.00	0.00	0.00	2.90	0.00	0.00	1.19
P (kW)	M	1999	4014	6005	6802	8004	8809	
	C	1977	3975	5988	6912	7997	8831	
	E	−1.09	−0.98	−0.28	1.62	−0.09	0.25	0.91
$p_{\max}$ (bar)	M	56	77	107	129	142	149	
	C	55.2	79.7	109.8	130.4	144.1	150.8	
	E	−3.16	2.18	1.67	0.31	0.77	0.53	1.75
$\dot{m}_{\text{az}}$ (kg/s)	M	4.75	9.17	13.7	-	16.0	-	
	C	4.88	9.26	13.8	14.5	16.4	17.3	
	E	2.68	0.96	1.02	-	2.38	-	1.94
T_e (K)	M	670	656	666	672	702	733	
	C	702	670	652	665	708	713	
	E	4.84	2.09	−2.12	−1.01	0.90	−2.76	2.62
T_m (K)	M	754	734	741	747	782	818	
	C	746	723	722	738	771	784	
	E	−1.06	−1.46	−2.56	−1.20	−1.43	−4.12	2.26
$\dot{m}_n$ (g/kWh)	M	16.72	9.04	8.90	-	11.02	-	
	C	19.04	10.15	9.46	18.58	11.08	15.56	
	E	13.09	12.27	6.34	-	0.51	-	9.79
RMSE		5.80	4.84	2.79	1.66	1.15	2.24	

From the view of the RMSE of each load, it can be observed that the 25% load has the largest root mean square error, followed by the 50% load. Under both loads, their RMSEs are significantly higher than the others. This fact indicates that the WA model is more accurate under moderate to heavy loads than under light loads. In general, the WA model provides a good performance prediction for all the parameters under all the loads.

The heat release characteristics of the engine with the WA model are presented in Figure 4. The trends of the heat release distribution and heat release rate are almost the same as those of the engine with the SL model. However, the values are different in the two models. The combustion duration at 25% load is almost equal to that at 100% load in the WA model. This may be unreasonable. At 25% load, more than 50% of the fuel burns in 25% time of combustion. At 100% load, approximately 30% of the fuel burns in 25% time of combustion.

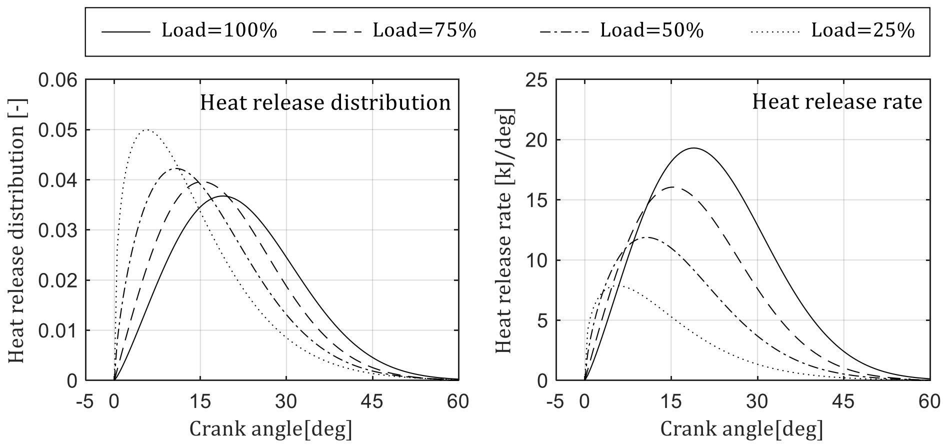

Figure 4. The heat release characteristics of the engine in liquid fuel mode with the WA model.

According to the curves of heat release rate, the heat release rate at 25% load is much greater than that at 100% load. It seems that combustion knock is apt to occur at 25% load rather than at 100% load. This contradicts the common principle of combustion. The heat release rate is proportional to the concentration of fuel and oxygen. The concentrations of fuel and oxygen at 25% load are lower than those at 100% load. The heat release rate at 25% load should be lower than that at 100% load.

5. Model Validation in Gas Fuel Mode

5.1. Wiebe Parameters according to the SL Model

The Wiebe parameters in gas fuel mode are given in Table 6. In gas fuel mode, the natural gas is injected at the intake port and ignited by the fuel oil. According to the document of this engine, both the natural gas injector and ignition injector are electronically controlled. As the flexibility feature of the electronic control system, the timing of ignition can be assigned to an arbitrary value in its control unit. The actual value of ignition timing depends entirely on the professionalism of the calibration engineer. Thus, the combustion beginning angle is derived from calibration. The other parameters are given according to our experience in model calibration and the rules we analyzed above.

Table 6. The Wiebe parameters according to the SL model in gas fuel mode.

Load (%)	25	50	75	85	100	110
φ_b (deg CA)	1	0	0	−3	−2	−2
φ_z (deg CA)	20	30	40	44	50	54
d (-)	1.1	1.0	0.9	0.86	0.8	0.76

5.2. Performance Validation of the SL Model

In gas fuel mode, the calculated engine performance and the actual engine performance are shown in Table 7 and Figure 5. At the 110% load and the 85% load, the emission performance rated parameters are not measured.

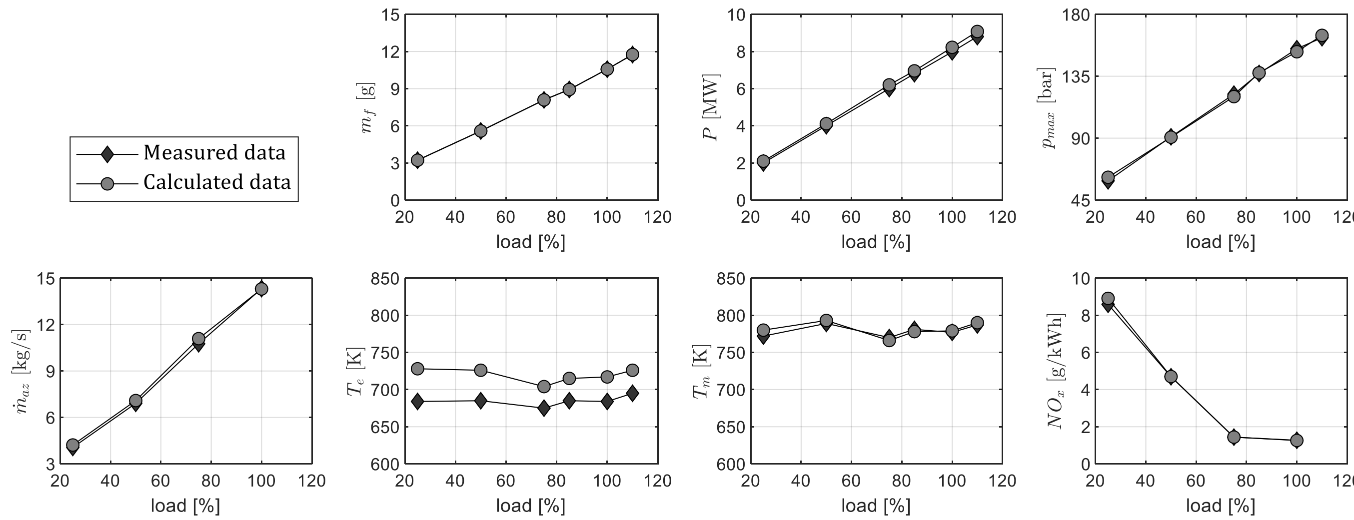

Figure 5. The calculated and measured results under gas fuel mode.

Table 7. The performance of the dual-fuel engine running in gas fuel mode with the SL model.

Load (%)		**25**	**50**	**75**	**85**	**100**	**110**	**RMSE**
m_f (g)	*M*	3.22	5.58	8.09	8.93	10.57	11.75	
	C	3.22	5.58	8.09	8.93	10.57	11.75	
	E	0.00	0.00	0.00	0.00	0.00	0.00	0.00
P (kW)	*M*	2000	4004	6003	6805	7981	8801	
	C	2096	4114	6204	6957	8224	9077	
	E	4.80	2.75	3.35	2.23	3.04	3.14	3.31
$p_{\max}$ (bar)	*M*	59	91	122	137	155	163	
	C	61.6	90.7	120.2	137.5	152.8	164.7	
	E	2.67	−1.41	−2.28	−0.36	−2.05	0.43	1.77
$\dot{m}_{az}$ (kg/s)	*M*	4.06	6.91	10.76	-	14.32	-	
	C	4.22	7.09	11.09	11.80	14.30	15.73	
	E	3.84	2.55	3.06	-	−0.14	-	2.82
T_e (K)	*M*	684	685	675	685	684	695	
	C	728	726	704	715	717	726	
	E	6.43	5.99	4.30	4.38	4.82	4.46	5.13
T_m (K)	*M*	772	789	770	781	777	787	
	C	780	793	766	778	779	790	
	E	1.04	0.51	−0.52	−0.38	0.26	0.38	0.57
$\dot{m}_n$ (g/kWh)	*M*	8.59	4.69	1.44	-	1.27	-	
	C	8.91	4.70	1.44	1.17	1.26	0.43	
	E	3.73	0.21	0.00	-	−0.79	-	1.91
RMSE		3.82	2.74	2.52	2.21	2.31	2.45	

The letters in Table 7 have the same meaning as those in Table 3, except for the mass of fuel m_f. In gas fuel mode, the value of m_f is an equivalent value for considering the pilot fuel. The pilot oil is converted to the mass of natural gas in terms of the same calorific value, as Equation (21) shows.

$$m_f = m_{f,NG} + \frac{m_{f,NG} \cdot LCV_{DO}}{LCV_{NG}} \tag{21}$$

According to the data in Table 7, the error between the calculated value and the measured value for all the parameters is almost within ±5%, except for the exhaust temperature T_e. The mass of the injected fuel under all the loads uses the measured value. For the engine power P, the maximum error is 4.80% at 25% load. For the peak firing pressure $p_{\max}$, it is 2.67% at 25% load. For the intake air mass flow rate $\dot{m}_{az}$, it is 3.84% at 25% load. For the exhaust temperature T_e, it is 6.43% at 25% load. For exhaust manifold temperature T_m, it is 1.04 at 25% load. For the NOx emission, it is 3.73% at 25% load. The excellent performance of the engine model indicates the feasibility of the SL model.

It also can be observed from the RMSEs of the parameters that the exhaust gas temperature has the largest RMSE. It reaches 5.13. The second largest is the shaft power of the engine. It is 3.31. This is followed by the mass flow rate of the intake air, at approximately 2.82. When we look at the RMSEs of the loads, the 25% load has the largest RMSE, approximately 3.82. From these analyses, it can be observed that the exhaust gas temperature shows the lowest accuracy for all the loads. This is because of the relatively poor accuracy of the exhaust gas temperature model. It can also be observed that the model shows better performance under moderate-to-heavy loads than under light loads. However, in general, the performance of the engine model is very good. The SL model presents high accuracy for all the parameters under all the loads.

By observing the curves in Figure 5 and the data in Table 7, it is found that the calculating error of the exhaust gas temperature T_e is significantly larger than that of other parameters. However, at the same time, the calculated exhaust manifold temperature T_m maintains high accuracy. The reason for that fact is the same as that which occurred in liquid fuel mode, which is caused by the error of the exhaust gas model itself. The injected gas mass m_f, the power P, the peak firing pressure $p_{\max}$, and the intake air flow rate $\dot{m}_{az}$ almost linearly increase with the increasing of load. The exhaust gas temperature and the exhaust manifold temperature do not change substantially as the load increases. The emission of the nitrogen oxide decreases when the load increases. However, it does not change monotonically with the load and shows irregularity. This is because the distribution of matter and temperature in the cylinder are too complicated. The simplified model cannot correctly obtain the key information regarding the quantity and the size of the high-temperature region.

The curves of the heat release distribution and the heat release rate of the dual-fuel engine running in gas fuel model are shown in Figure 6. Similar to the liquid fuel mode, all the curves are shifted to the zero crank angle. When the load increases, the fraction of initial burned fuel decreases, but the heat release rate remains almost the same in the first five crank angles. As the load increases, the increase rate of maximum heat release rate decreases. Compared with the liquid fuel mode, in gas fuel mode, the beginning curve of the heat release rate is much steeper. This is consistent with the fact that in gas fuel mode engine, it is more prone to combustion knock than in liquid fuel mode. These characteristics of the curves align with the trend of the actual combustion well.

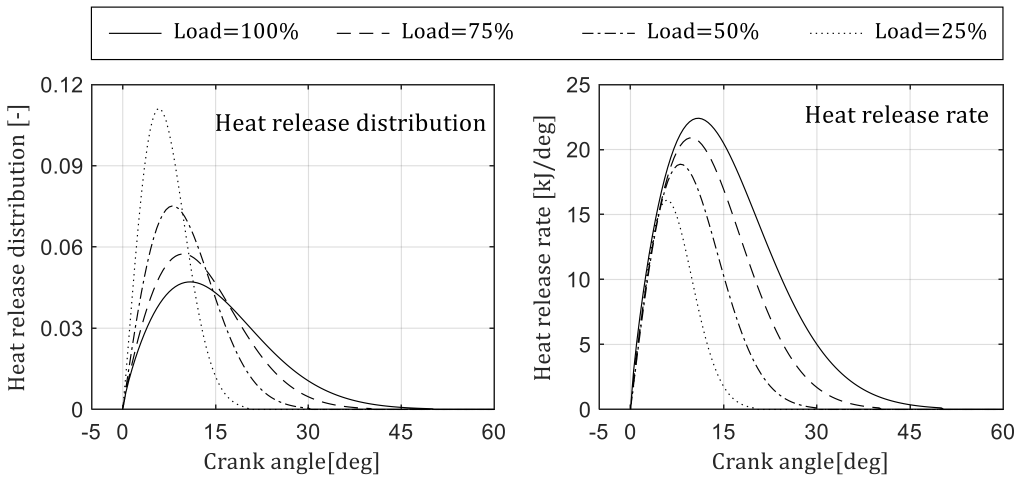

Figure 6. The heat release characteristics of the engine in gas fuel mode with the SL model.

5.3. Further Discussion of the Woschni/Anisits Model

Since there is no well-known Wiebe parameters model for the gas engine, the WA model is also used. The combustion beginning angles and the Wiebe parameters at 100% load are the same as those in the SL model. Other Wiebe parameters are calculated by the WA model, as shown in Table 8.

Table 8. The Wiebe parameters according to the WA model in gas fuel mode.

Load (%)	25	50	75	85	100	110
α (-)	2.20	2.05	2.26	2.18	2.24	2.23
p (bar)	1.15	1.81	2.75	2.92	3.54	3.88
T (K)	378	362	358	356	356	356
τ_{ID_0}/τ_{ID} (-)	1	1	1	1	1	1
φ_b (CA)	1	0	0	−3	−2	−2
φ_z (CA)	50.6	52.7	49.7	50.8	50.0	50.1
d (-)	0.24	0.40	0.62	0.66	0.80	0.88

The air–fuel equivalence ratio is calculated by Equation (22). Other parameters are obtained in the same way as those in liquid fuel mode. It can be seen from Table 8 that the calculated combustion durations under all the loads are almost the same. The combustion distribution factor d increases along with the loads.

$$\alpha = \frac{\dot{m}_a}{\dot{m}_f \times 17.4} \tag{22}$$

To validate the model performance, the calculated engine performance is presented in Table 9. In Table 9, the measured pressure is the gauge pressure, but the calculated value is the absolute pressure. The specific mass flow rate of NOx shows the poorest performance. Its error is −65.54% at 25% load and −53.73% at 50% load. Its RMSE for all the loads is 45.20. It is much higher than other parameters. The second highest is the exhaust gas temperature, followed by the peak firing pressure. The peak firing pressure $p_{\max}$ and the exhaust manifold temperature T_m reveal apparent deterioration at 25% load. It is approximately 6 times and approximately 15 times the errors at 100% load, respectively. The engine power P and the intake air mass flow $\dot{m}_{az}$ have good accuracy under all the loads, nearly within 2%. When we investigate the data from the RMSEs of loads, it can be seen that the RMSEs at 25% load and at 50% load are much larger than those under other loads.

Table 9. The performance of the dual-fuel engine running in gas fuel mode with the WA model.

Load (%)		**25**	**50**	**75**	**85**	**100**	**110**	**RMSE**
m_f (g)	M	3.22	5.58	8.09	8.93	10.57	11.75	
	C	3.22	5.58	8.09	8.93	10.57	11.75	
	E	0.00	0.00	0.00	0.00	0.00	0.00	0.00
P (kW)	M	2000	4004	6003	6805	7981	8801	
	C	2036	4058	6157	6923	8224	9100	
	E	1.80	1.35	2.57	1.73	3.04	3.40	2.43
$p_{\max}$ (bar)	M	59	91	122	137	155	163	
	C	52.8	85.9	117.8	136.2	152.8	164.6	
	E	−12.00	6.63	−4.23	−1.30	−2.05	0.37	5.94
$\dot{m}_{\mathrm{az}}$ (kg/s)	M	4.06	6.91	10.76	-	14.32	-	
	C	4.13	7.09	11.09	11.80	14.30	15.73	
	E	1.63	2.55	3.06	-	−0.14	-	2.19
T_e (K)	M	684	685	675	685	684	695	
	C	745	732	707	717	717	725	
	E	8.92	6.86	4.74	4.67	4.82	4.32	5.96
T_m (K)	M	772	789	770	781	777	787	
	C	803	801	770	780	779	789	
	E	4.02	1.52	0.00	−0.13	0.26	0.25	1.76
$\dot{m}_n$ (g/kWh)	M	8.59	4.69	1.44	-	1.27	-	
	C	2.96	2.17	1.02	1.09	1.12	0.44	
	E	−65.54	−53.73	−29.17	-	−11.81	-	45.20
RMSE		25.47	20.66	11.38	2.30	5.02	2.46	

From the above analysis, it can be seen that the thermal parameters are calculated well by the engine model with WA model, but the emission parameter is poor. The WA model can also be used for gas fuel mode of the dual-fuel engine, but the accuracy is not good. Thus, it is not recommended for the calculation of NOx emission.

The curves of the heat release distribution and the heat release rate of the engine running in gas fuel mode with the WA model are presented in Figure 7. The characteristics of heat release are similar to the WA model in liquid fuel mode. Its change trends of the heat release distribution and heat release rate are consistent with SL model, but the values are very different. The 25% load has the sharpest rising rate, almost vertical, in the curves of heat release distribution. This indicates that the initial combustion fuel takes account of the majority of the total fuel. In the curves of the heat release rate, the 25% load has the highest heat release rate at the beginning of combustion. These results are inconsistent with the actual characteristics of combustion. The combustion rate at 25% load should be the lowest. The combustion rate is proportional to the fuel concentration and oxygen concentration. At 25% load, the fuel concentration is much less than the 100% load. The oxygen concentration is also a little lower than that at 100% load.

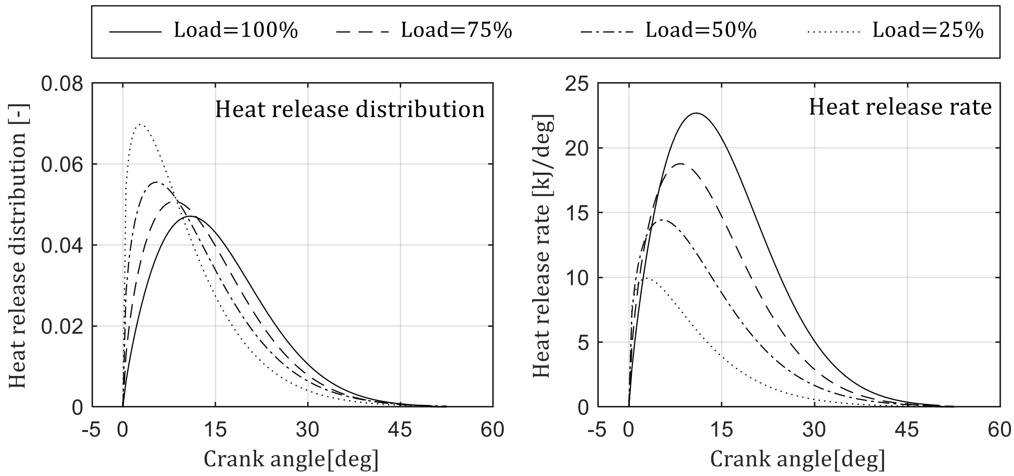

Figure 7. The heat release characteristics of the engine in gas fuel mode with WA model.

6. Model Validation in Fuel Sharing Mode

6.1. The Four Types of Combinations

The heat release rate in fuel sharing mode is derived from the models in liquid fuel mode and gas fuel mode. In this study, four types of combinations are investigated.

In Case 1, the Wiebe mode in fuel sharing mode is the linear combination of heat release in gas fuel mode and liquid fuel mode. Therefore, the released heat is obtained according to Equation (23).

$$\frac{dQ_{\mathrm{s}}}{d\varphi} = \frac{dQ_{\mathrm{g}}}{d\varphi} \times w_{\mathrm{g}} + \frac{dQ_{l}}{d\varphi} \times \left(1 - w_{\mathrm{g}}\right) \tag{23}$$

The Q is the released heat. Subscript s stands for fuel sharing mode, g stands for gas fuel mode, and l stands for liquid fuel mode. w_{g} is the energy fraction of natural gas to the total energy. w_{g} is derived by Equation (24). The LHV is the lower heating value of the fuel.

$$w_{\mathrm{g}} = \frac{m_{\mathrm{g}} \times LHV_{\mathrm{g}}}{m_{\mathrm{g}} \times LHV_{\mathrm{g}} + m_{l} \times LHV_{l}} \tag{24}$$

In Case 2, the Wiebe parameters in fuel sharing mode are the linear combination of Wiebe parameters in gas fuel mode and liquid fuel mode, as Equation (25) shows.

$$\begin{cases} d_{\mathrm{s}} = d_{\mathrm{g}} \times w_{\mathrm{g}} + d_{l} \times \left(1 - w_{\mathrm{g}}\right) \\ \varphi_{\mathrm{z,s}} = \varphi_{\mathrm{z,g}} \times w_{\mathrm{g}} + \varphi_{\mathrm{z},l} \times \left(1 - w_{\mathrm{g}}\right) \\ \varphi_{\mathrm{b,s}} = \varphi_{\mathrm{b,g}} \times w_{\mathrm{g}} + \varphi_{\mathrm{b},l} \times \left(1 - w_{\mathrm{g}}\right) \end{cases} \tag{25}$$

In Case 3, the timing of combustion beginning is assumed to be governed by the main injector. Therefore, we assumed that the combustion beginning angle is the same as the value in liquid fuel mode, but other parameters are the same as those in Case 2. In Case 4, the timing of combustion beginning is the same as the value in gas fuel mode, but other parameters are the same as those in Case 2.

For comparison, two fine calibration cases are added. As the timing in fuel sharing mode is difficult to determine, in Case 5 only the timing of combustion beginning is tuned with the target of minimizing the overall RMSE. Other parameters in Case 5 are the same as those in Case 2. In Case 6, all the parameters except the Wiebe parameters are calibrated. All the Wiebe parameters are shown in Table 10.

Table 10. The Wiebe parameters according to the SL model in fuel sharing mode.

Case (-)	1	2	3	4	5	6
φ_b (deg CA)	-	−3.7	−4.4	−3.0	−2.8	−3.2
φ_z (deg CA)	-	49.3	49.3	49.3	49.3	49.3
d (-)	-	1.07	1.07	1.07	1.07	1.07

The engine model runs on Boost. However, the dual-fuel combustion model is not provided on Boost. The HRR is the final value used by Boost for combustion calculation regardless of whether it is derived from the diesel combustion model, the gas combustion model, or the fuel sharing combustion model. On the basis of that fact, in Case 1, the HRR Table is used, which is more convenient than using a double-Wiebe model. The HRR values are derived according to Equation (23). For Case 2 to Case 6, the Wiebe model is still used.

6.2. Performance Validation of the SL Model

The calculated parameters are presented in Table 11. As in fuel sharing mode, only the engine running at the 85% load is tested, and all six cases are also only calculated at 85% load. The mass of injected fuel at Case 6 is a corrected value, at other cases, it is the measured value. For the overall engine performances of the four types of combinations, the RMSE of Case 3 is the highest, reaching 3.09. The second is Case 1, approximately 2.75. Then, it is Case 2, at approximately 2.53. The last is Case 4, at approximately 2.31.

Table 11. The performance of the dual-fuel engine running in fuel sharing mode with the SL model.

Case (-)		1	2	3	4	5	6	M
m_f (g)	V	143	143	143	143	143	140	143
	E	0.00	0.00	0.00	0.00	0.00	−2.10	-
P (kW)	V	7132	7122	7150	7092	7083	6944	6802
	E	4.85	4.70	5.12	4.26	4.13	2.09	-
$p_{\max}$ (bar)	V	129.1	127.6	130.4	124.7	123.9	124.5	125
	E	2.46	1.27	3.49	−1.03	−1.67	−1.19	-
T_e (K)	V	736.3	736.4	734.5	738.2	739.0	730.0	727
	E	1.28	1.29	1.03	1.54	1.65	0.41	-
T_m (K)	V	805.8	805.6	803.3	808.2	809.0	797.0	827
	E	−2.56	−2.59	−2.87	−2.27	−2.18	−3.63	-
RMSE (-)		2.75	2.53	3.09	2.31	2.34	2.17	-

From the above analysis, it is shown that Case 4 obtains the best overall performance among the four types of combinations. In fact, Case 2 and Case 1 are also very accurate, but the model of Case 1 is not consistent with the models of liquid fuel model and gas fuel model in form. The combustion beginning angle of Case 5 is fine-tuned. It should have a better performance than Case 4. However, Case 5 even shows a slightly poorer performance than Case 4. In fact, it is difficult to tune even better Wiebe parameters artificially. This result indicates that the SL model is able to generate better Wiebe parameters than the manually tuned Wiebe parameters. When the cost of model calibration is considered, the derived combustion beginning from liquid fuel mode and gas fuel mode in Case 2 is a good choice. Case 6 has the lowest RMSE owing to the fine-tuning of parameters except for the Wiebe parameters. The RMSE of Case 6 improves 0.14 compared with the RMSE of case 4, which improves 0.36 compared with the RMSE of Case 2. Therefore, from the above analysis, it can be inferred that Case 2 and Case 4 are the best two types of combination for fuel sharing mode. For better robustness and experience, Case 2 is recommended.

6.3. Further Discussion of the Woschni/Anisits Model

To investigate the performance of the Woschni/Anisits model, the first five cases with the data from the WA model are calculated again. Case 6 retains the same parameters as that in SL model. The Wiebe parameters are presented in Table 12. Case 1 uses the heat release table. Its value is the combination of the released heat in liquid fuel mode and in gas fuel mode directly. The table is not applicable to Case 1.

Table 12. The Wiebe parameters according to the WA model in fuel sharing mode.

Case (-)	**1**	**2**	**3**	**4**	**5**	**6**
φ_b (deg CA)	-	−3.7	−4.4	−3.0	−2.8	−3.2
φ_z (deg CA)	-	55.3	55.3	55.3	55.3	49.3
d (-)	-	0.87	0.87	0.87	0.87	1.07

The engine performance of the six cases is presented in Table 13. On the whole, the RMSEs of the first five cases are slightly better than those in the SL model. The largest RMSE occurs in Case 3. Its value is 2.58. It is 0.51 lower than the biggest RMSE in SL model, which also occurs in Case 3. Case 2 shows the best RMSE among the four types of combinations, i.e., the first four cases. Its value is 2.19. It is 0.01 greater than the RMSE of Case 6, the carefully tuned case. It is 0.1 smaller than the RMSE of Case 5. The second best RMSE occurs in Case 4. It is 0.02 lower than the RMSE of Case 2. Therefore, from the above analysis, it also can be concluded that Case 2 and Case 4 are also the best two types of combination for fuel sharing mode. This is consistent with the results from SL model. For better robustness and experience, Case 2 is recommended.

Table 13. The performance of the dual-fuel engine running in liquid fuel mode with the WA model.

Case (-)		**1**	**2**	**3**	**4**	**5**	**6**	**M**
m_f (g)	V	143	143	143	143	143	140	143
	E	0.00	0.00	0.00	0.00	0.00	0.00	-
P (kW)	V	7100	7079	7106	7050	7041	6944	6802
	E	4.38	4.07	4.47	3.65	3.51	2.09	-
$p_{\max}$ (bar)	V	128.8	126.2	128.9	123.5	122.7	124.5	125
	E	2.22	0.16	2.30	−1.98	−2.62	−0.40	-
T_e (K)	V	738.1	738.6	736.7	740.8	741.1	730.0	727
	E	1.53	1.60	1.33	1.90	1.94	0.41	-
T_m (K)	V	808.1	808.7	806.2	811.4	812.2	797.0	827
	E	−2.29	−2.21	−2.52	−1.89	−1.79	−3.63	-
RMSE (-)		2.52	2.19	2.58	2.21	2.29	2.18	-

7. Summary

Under our hypothesis, the Wiebe parameters are given, and the performance calculated by the engine model is checked to be well matched with the performance of the actual engine, according to the validated Wiebe parameters in liquid fuel mode, gas fuel mode, and fuel sharing mode. The SL model can be rewritten as Equations (26)–(28).

$$\varphi_z = w_g \times \varphi_{z0} \times \left(0.7 \times \frac{m_f}{m_{f0}} + 0.3\right) + (1 - w_g) \times \left[\varphi_{z0} \times \left(0.7 \times \frac{m_f}{m_{f0}} + 0.3\right) - 10\right] \quad (26)$$

$$d = w_g \times d_0 \times \left(-0.35 \times \frac{m_f}{m_{f0}} + 1.35\right) + (1 - w_g) \times \left[d_0 \times \left(-0.35 \times \frac{m_f}{m_{f0}} + 1.35\right) - 0.4\right] \quad (27)$$

$$\varphi_b = w_g \times f_{3l}(P_{load}) + (1 - w_g) \times f_{3g}(P_{load}) \quad (28)$$

The Wiebe parameters calculated by the SL model are well consistent with the validated Wiebe parameters in all operating modes and loads, as shown in Figure 8. All the calibrated values and the model calculated values are normalized according to the corresponding reference values. The results of the engine performance that have been discussed in liquid fuel mode, gas fuel mode, and fuel sharing mode prove that the SL model is able to generate an accurate dual-fuel engine model.

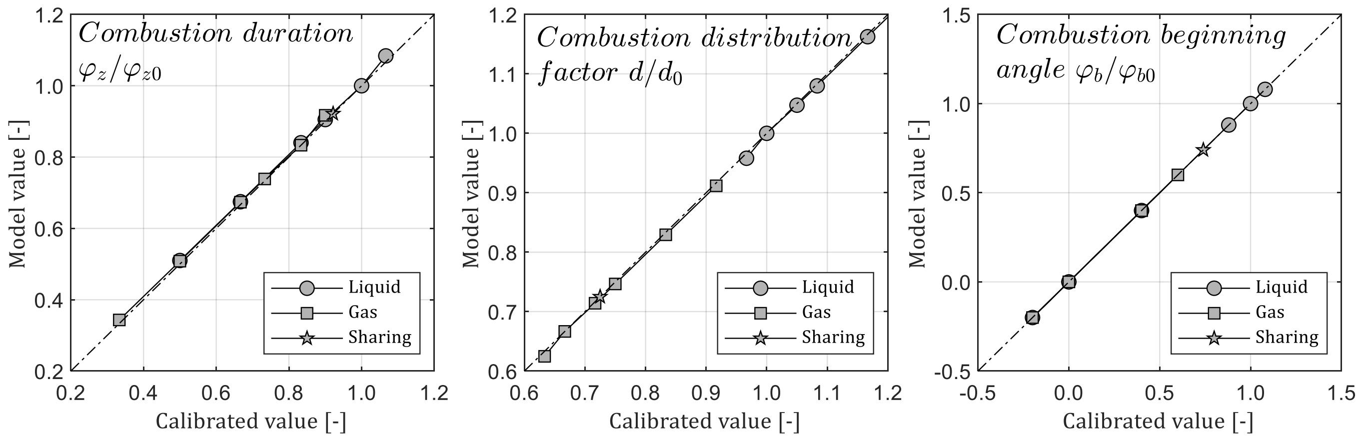

Figure 8. The calculated values from the SL model and the calibrated Wiebe parameters.

8. Conclusions

In our simulator development, there is a fixed-speed four-stroke NG-diesel dual-fuel engine that is able to run in liquid fuel mode, gas fuel mode, fuel sharing mode, and backup mode. As the current control-oriented heat release rate model is specifically used for diesel engines or gasoline engines or gas engines, there is a lack of a commonly accepted heat release model that can be used for the dual-fuel engine operating at all the modes and loads. On the basis of our experience and practice, a Wiebe-based heat release rate model is used. In order to make the Wiebe model available for the dual-fuel engine, the Wiebe parameters are assumed to be linear functions, and they are modeled. To validate our hypothesis and models, the Wiebe parameters in liquid fuel mode and gas fuel mode are given, four types of combinations in fuel sharing model are discussed, and the engine performance is checked and analysed. Results show that the proposed SL model is a well-performing model. The following conclusions can be derived from this study.

The proposed SL model shows high accuracy and can be used for control-oriented dual-fuel engine models. In the liquid fuel mode, the errors of all the parameters are within $\pm 4\%$, and many are even within $\pm 1\%$. Its average RMSE is 1.45% for all the considered loads. In the gas fuel mode, the errors of almost all the parameters are within $\pm 5\%$. Its average RMSE is 2.22% for all the considered loads. In the fuel sharing mode, the errors of all the parameters are within $\pm 5\%$ for Case 2. Its RMSE is 2.53%. For the fixed-speed four-stroke NG-diesel dual fuel engine, the Wiebe parameters can be modeled as a linear function. The SL model is accurate for control-oriented applications.

The SL model is able to generate Wiebe parameters that are better than the carefully tuned parameters. In fuel sharing mode, four types of combinations and two cases of comparisons are investigated. For the four types of combinations, the heat release rate in fuel sharing mode is derived from the heat release rate models in liquid fuel mode and gas fuel mode. For Case 5 and Case 6, the heat release rate in fuel sharing mode is derived separately from the carefully tuned Wiebe parameters and carefully tuned engine parameters. For the SL model, the RMSE of Case 4 is 0.03% lower than that in case 5. For the WA model, the RMSE of Case 4 is 0.08% lower than that in Case 5, and the RMSE of Case 2 is 0.10% lower than that in Case 5. The model generated Wiebe parameters are comparable to the carefully tuned Wiebe parameters.

The WA model is not suitable for engine models that require NOx-emission-related parameters. In the liquid fuel mode, the errors of the NOx emission are within ±14%, and other thermal parameters are within ±5%. Its average RMSE is 2.92% for all the considered loads. The RMSE of the NOx emission is 9.79%. For other thermal parameters, it is within 6%. In the gas fuel mode, the errors of the NOx emission are within ±66%, and other thermal parameters are within ±12%. Its average RMSE is 9.07% for all the considered loads. The RMSE of the NOx emission is 45.20%. For other thermal parameters, it is within 6%. The error of NOx emission is much higher than that of the other parameters. This is the result of the inappropriate heat release rate model.

Author Contributions: Y.T., conceptualization, methodology, software, writing—original draft preparation, investigation, and validation; H.L., data curation, visualization, and software; Y.J., visualization and formal analysis; W.L., writing—review and editing; J.Z., supervision and validation. All authors have read and agreed to the published version of the manuscript.

Funding: This study is financially supported by the National Natural Science Foundation of China (Grant No. 52071090), China Postdoctoral Science Foundation (Grant No. 2021M690495), and the Fundamental Research Funds for the Central Universities (Grant No. 017200221).

Institutional Review Board Statement: Not applicable.

Informed Consent Statement: Not applicable.

Data Availability Statement: Data are available within this article.

Conflicts of Interest: The authors declare that they have no known competing financial interests or personal relationships that could have appeared to influence the work reported in this paper.

Nomenclature

$\varphi_b{}'$	Combustion beginning angle before correction (degree of crank angle)
φ_b	Combustion beginning angle (degree of crank angle)
φ_z	Combustion duration (degree of crank angle)
φ_{z0}	Combustion duration at the reference working condition (degree of crank angle)
d	Combustion distribution factor (-)
d_0	Combustion distribution factor at the reference working condition (-)
m_f	Mass of fuel injected into cylinder (g)
m_{f0}	Mass of injected fuel at the reference working condition (g)
P	Shaft power of engine (kW)
$p_{\max}$	The peak firing pressure of cylinder (bar)
$\dot{m}_{\mathrm{az}}$	The gross mass flow rate from intake manifold into cylinder (kg/s)
T_e	Exhaust gas temperature (K)
T_m	The temperature of exhaust manifold (K)
$\dot{m}_n$	The specific mass flow rate of nitrogen oxide (g/kWh)
α	The air–fuel equivalence ratio (-)
p	Pressure at the beginning of compression stroke (bar)
T	Temperature at the beginning of compression stroke (K)
τ_{ID}	Ignition delay (degree of crank angle)
w_{g}	Weight fraction between the energy of natural gas and the total energy (-)

Abbreviations

SL	Our proposed standard linear model
WA	A version of SL, where φ_z and d are calculated by the Woschni/Anisits model
RMSE	Root mean square error
NG	Natural gas
LNG	Liquified natural gas
GHG	Greenhouse gas
MCC	Mixing-controlled combustion
DI	Direct injection
0D	Zero-dimension
HCCI	Homogeneous charge compression ignition
RCCI	Reactivity-controlled compression ignition
VGT	Variable geometry turbocharger
VIT	Variable injection timing
EGR	Exhaust gas recirculation
LCF	Load correction factor
OCF	Oxygenate correction factor
LR	Lloyd's Register of Shipping
CCS	China Classification Society
RINA	Registro Italiano Navale

References

1. MEPC. *Meeting Summary of the Marine Environment Protection Committee (MEPC), 72nd Session*; MEPC: London, UK, 2018.
2. Zamboni, G. A Study on Combustion Parameters in an Automotive Turbocharged Diesel Engine. *Energies* **2018**, *11*, 2531. [CrossRef]
3. Ambrozik, T. The methodology of heat release characteristics determination on the basis of the real indicator diagram. *Heat Transf. Res.* **2018**, *49*, 1629–1644. [CrossRef]
4. Pashaei, J.; Saray, R.K. Development of a quasi-dimensional, fractal-base combustion model for SI engines by simulating flame-wall interaction phenomenon. *Fuel* **2019**, *236*, 13–29. [CrossRef]
5. Feng, Y.M.; Wang, H.Y.; Gao, R.F.; Zhu, Y.Q. A Zero-Dimensional Mixing Controlled Combustion Model for Real Time Performance Simulation of Marine Two-Stroke Diesel Engines. *Energies* **2019**, *12*, 2000. [CrossRef]
6. Dowell, P.G.; Akehurst, S.; Burke, R.D. A real-time capable mixing controlled combustion model for highly diluted conditions. *Energy* **2017**, *133*, 1035–1049. [CrossRef]
7. Smith, J.K.; Roberts, P.; Kountouriotis, A.; Richardson, D.; Aleiferis, P.; Ruprecht, D. Thermodynamic modelling of a stratified charge spark ignition engine. *Int. J. Engine Res.* **2020**, *21*, 801–810. [CrossRef]
8. Kim, M.; Kim, Y.; Kim, J.; Song, H.H. Development of quasi-dimensional turbulence model for spark-ignition engine with physical analysis of tumble: Energy-based tumble model focusing on energy intake and turbulence production. *Appl. Energy* **2019**, *252*, 113455. [CrossRef]
9. Ghojel, J.I. Review of the development and applications of the Wiebe function: A tribute to the contribution of Ivan Wiebe to engine research. *Int. J. Engine Res.* **2010**, *11*, 297–312. [CrossRef]
10. Giacomazzi, E.; Bruno, C.; Favini, B. Fractal modelling of turbulent combustion. *Combust. Theory Model.* **2000**, *4*, 391–412. [CrossRef]
11. Xu, S.N.; Yamakawa, H.; Nishida, K.; Filipi, Z. Quasi-Dimensional Diesel Engine Combustion Modeling with Improved Diesel Spray Tip Penetration, Ignition Delay, and Heat Release Submodels. *J. Eng. Gas Turbines Power Trans. Asme* **2017**, *139*, 1–17. [CrossRef]
12. Tang, Y.; Zhang, J.; Gan, H.; Jia, B.; Xia, Y. Development of a real-time two-stroke marine diesel engine model with in-cylinder pressure prediction capability. *Appl. Energy* **2017**, *194*, 55–70. [CrossRef]
13. Zhou, Y.C.; Hariharan, D.; Yang, R.N.; Mamalis, S.; Lawler, B. A predictive 0-D HCCI combustion model for ethanol, natural gas, gasoline, and primary reference fuel blends. *Fuel* **2019**, *237*, 658–675. [CrossRef]
14. Wu, Y.Y.; Wang, J.H.; Mir, F.M. Improving the Thermal Efficiency of the Homogeneous Charge Compression Ignition Engine by Using Various Combustion Patterns. *Energies* **2018**, *11*, 3002. [CrossRef]
15. Kakoee, A.; Bakhshan, Y.; Barbier, A.; Bares, P.; Guardiola, C. Modeling combustion timing in an RCCI engine by means of a control oriented model. *Control Eng. Pract.* **2020**, *97*, 104321. [CrossRef]
16. Yang, T.H.; Yin, L.H.; Meng, X.Y.; Tian, H.; Long, W.Q.; Tunestal, P. Partially premixed combustion optimization using double injection strategy in transient operation. *Appl. Therm. Eng.* **2020**, *169*, 114963. [CrossRef]
17. Novaes, T.; Henriquez, J.R.; Ochoa, A.A.V. Numerical simulation of the performance of a diesel cycle operating with diesel-biodiesel mixtures. *Energy Convers. Manag.* **2019**, *180*, 990–1000. [CrossRef]

18. Sapra, H.; Godjevac, M.; De Vos, P.; Van Sluijs, W.; Linden, Y.; Visser, K. Hydrogen-natural gas combustion in a marine lean-burn SI engine: A comparitive analysis of Seiliger and double Wiebe function-based zero dimensional modelling. *Energy Convers. Manag.* **2020**, *207*, 112494. [CrossRef]
19. Diaz, G.J.A.; Montoya, J.P.G.; Martinez, L.A.C.; Olsen, D.B.; Navarro, A.S. Influence of engine operating conditions on combustion parameters in a spark ignited internal combustion engine fueled with blends of methane and hydrogen. *Energy Convers. Manag.* **2019**, *181*, 414–424. [CrossRef]
20. Shibata, G.; Ogawa, H.; Amanuma, Y.; Okamoto, Y. Optimization of multiple heat releases in pre-mixed diesel engine combustion for high thermal efficiency and low combustion noise by a genetic-based algorithm method. *Int. J. Engine Res.* **2019**, *20*, 540–554. [CrossRef]
21. Sui, W.B.; Hall, C.M.; Kapadia, G. Cylinder-specific model-based control of combustion phasing for multiple-cylinder diesel engines operating with high dilution and boost levels. *Int. J. Engine Res.* **2020**, *21*, 1231–1250. [CrossRef]
22. Sui, W.B.; Hall, C.M. Combustion phasing modeling and control for compression ignition engines with high dilution and boost levels. *Proc. Inst. Mech. Eng. Part D J. Automob. Eng.* **2019**, *233*, 1834–1850. [CrossRef]
23. Sui, W.B.; Gonzalez, J.P.; Hall, C.M. Modeling and Control of Combustion Phasing in Dual-Fuel Compression Ignition Engines. *J. Eng. Gas Turbines Power Trans. Asme* **2019**, *141*, 051005. [CrossRef]
24. Xiang, L.; Theotokatos, G.; Cui, H.N.; Xu, K.D.; Ben, H.K.; Ding, Y. Parametric Knocking Performance Investigation of Spark Ignition Natural Gas Engines and Dual Fuel Engines. *J. Mar. Sci. Eng.* **2020**, *8*, 459. [CrossRef]
25. Gutierrez, R.H.R.; Belchior, C.R.P.; Vaz, L.A.; Monteiro, U.A. Diagnostic methodology in four-stroke marine diesel engine by identifying operational parameters. *J. Braz. Soc. Mech. Sci. Eng.* **2018**, *40*, 500. [CrossRef]
26. Bondarenko, O.; Fukuda, T. Development of a diesel engine's digital twin for predicting propulsion system dynamics. *Energy* **2020**, *196*, 117126. [CrossRef]
27. Wang, L.; Zhao, Z.F.; Zhang, S.L.; Yu, C.C. Predictions of the heat release rate model of hydraulic-free piston engines. *Appl. Therm. Eng.* **2018**, *144*, 522–531. [CrossRef]
28. Liu, J.L.; Dumitrescu, C.E. Improved Thermodynamic Model for Lean Natural Gas Spark Ignition in a Diesel Engine Using a Triple Wiebe Function. *J. Energy Resour. Technol. Trans. Asme* **2020**, *142*, 062303. [CrossRef]
29. Liu, J.L.; Dumitrescu, C.E. Single and double Wiebe function combustion model for a heavy-duty diesel engine retrofitted to natural-gas spark-ignition. *Appl. Energy* **2019**, *248*, 95–103. [CrossRef]
30. Kozlov, A.; Grinev, V.; Terenchenko, A.; Kornilov, G. An Investigation of the Effect of Fuel Supply Parameters on Combustion Process of the Heavy-Duty Dual-Fuel Diesel Ignited Gas Engine. *Energies* **2019**, *12*, 2280. [CrossRef]
31. Mikulski, M.; Wierzbicki, S. Validation of a zero-dimensional and two-phase combustion model for dual-fuel compression ignition engine simulation. *Therm. Sci.* **2017**, *21*, 387–399. [CrossRef]
32. Mikulski, M.; Wierzbicki, S.; Piętak, A. Verification of a 2–Phase, Zero-Dimensional Model of a Multifuel Compression-Ignition Engine in Single Fuel Operation. *Appl. Mech. Mater.* **2016**, *817*, 47–56. [CrossRef]
33. Loganathan, S.; Martin, M.L.J.; Nagalingam, B.; Prabhu, L. Heat release rate and performance simulation of DME fuelled diesel engine using oxygenate correction factor and load correction factor in double Wiebe function. *Energy* **2018**, *150*, 77–91. [CrossRef]
34. Stoumpos, S.; Theotokatos, G.; Mavrelos, C.; Boulougouris, E. Towards Marine Dual Fuel Engines Digital Twins-Integrated Modelling of Thermodynamic Processes and Control System Functions. *J. Mar. Sci. Eng.* **2020**, *8*, 200. [CrossRef]
35. Blomberg, C.K.; Wright, Y.M.; Boulouchos, K. A phenomenological HCCI combustion model in 0D and 3D-CFD. *Fuel* **2018**, *226*, 365–380. [CrossRef]
36. Tolou, S.; Vedula, R.T.; Schock, H.; Zhu, G.M.; Sun, Y.; Kotrba, A. Combustion Model for a Homogeneous Turbocharged Gasoline Direct-Injection Engine. *J. Eng. Gas Turbines Power Trans. Asme* **2018**, *140*, 102804. [CrossRef]
37. Xiang, L.; Song, E.Z.; Ding, Y. A Two-Zone Combustion Model for Knocking Prediction of Marine Natural Gas SI Engines. *Energies* **2018**, *11*, 561. [CrossRef]
38. Vihar, R.; Baskovic, U.Z.; Katrasnik, T. Real-time capable virtual NOx sensor for diesel engines based on a two-zone thermodynamic model. *Oil Gas Sci. Technol. Rev. D Ifp Energ. Nouv.* **2018**, *73*, 11. [CrossRef]
39. Tang, Y.; Zhang, J.; Jia, B.; He, Z.; Xia, Y. Investigation on the solution of nitric oxide emission model for diesel engine using optimization algorithms. *Fuel* **2018**, *228*, 81–91. [CrossRef]
40. Tang, Y.; Zhang, J.; Jia, B.; Sheng, H. Investigating the effect of cylinder body on the accuracy of marine diesel engine model. *J. Harbin Eng. Univ.* **2017**, *38*, 1836–1849.